Characterization of a Gas-Liquid OBC: Bubble Size and Gas Holdup

Mónica S. N. Oliveira and Xiong-Wei Ni
Centre for Oscillatory Baffled Reactor Applications (COBRA), Chemical Engineering, School of Engineering and Physical Sciences Heriot-Watt University, Riccarton, Edinburgh, EH14 4AS, U.K.

DOI 10.1002/aic.10282
Published online in Wiley InterScience (www.interscience.wiley.com).

A fundamental experimental study of gas-liquid contacting in an oscillatory baffled column is presented focusing on the effect of fluid oscillation on gas holdup and bubble size. The results show that beyond a critical level of fluid oscillation the Sauter mean diameter of the dispersion is substantially reduced, while the gas holdup (and, thus, the residence time of the gas phase) increases significantly. The reduction of bubble size was described in terms of bubble breakage, caused by the interaction of the bubbles with eddies. The experimental results were modeled by applying Kolmogoroff's theory of isotropic turbulence. The steep increase in the gas holdup with oscillation was mainly due to bubble entrainment by large vortices, formed by the oscillatory flow in the presence of baffles. A semi-theoretical expression, based on the forces acting on a bubble, was proposed, and was able to accurately match the experimental trends. The results also show that the gas-liquid hydrodynamics are mainly governed by the oscillatory operating conditions, and independent of the type of gas sparger. © 2004 American Institute of Chemical Engineers *AIChE J,* 50: 3019–3033, 2004
Keywords: Oscillatory baffled column, bubble size, bubble breakage, gas holdup, vorticity, hydrodynamics

Introduction

Early research into the effects of oscillatory flow in furrowed and wavy channels (Stephanoff et al., 1980) and around sharp edges (Knott and Mackley, 1980) showed that significant vortex formation and mixing could be obtained. In particular, Brunold et al. (1989) found that oscillatory flow in a tube with periodically spaced single-orifice baffles generated a complex flow pattern with intense eddy mixing. These studies have led to the development of the oscillatory baffled column (OBC), which has since been applied to numerous chemical engineering processes (see Ni et al. (2003a) for a review).

In an OBC, the fluid is periodically oscillated in the axial direction inside a cylindrical tube containing evenly spaced orifice baffles. The presence of baffles positioned transversely to the oscillating flow induces the formation of eddies, which are responsible for the highly chaotic nature of the flow (Roberts and Mackley, 1996). The development of the flow in an OBC during the upstroke of oscillation is shown in Figure 1. At the start of the upstroke (Figure 1a), vortices begin to form adjacent to the downstream edge of the baffles, and become fully developed at the point of maximum oscillatory velocity (Figure 1b). As the flow decelerates, the vortices are swept into the bulk of the baffled cell (Figure 1c) and reach the center of the cell at the point of flow reversal (Figure 1d). As the downstroke begins, these vortices unravel while new vortices are formed on the opposite edge of the baffle. The cycle then repeats itself in the opposite direction of flow. This mechanism has been observed in flow visualization studies (Brunold et al., 1989), measured by particle image velocimetry (Ni et al., 1995b) and predicted by numerical simulations (Howes et al., 1991). The flow is axisymmetric at low amplitudes and frequencies, but becomes chaotic as the intensity of oscillation increases (Roberts and Mackley, 1996).

Correspondence concerning this article should be addressed to X. W. Ni at x.ni@hw.ac.uk.

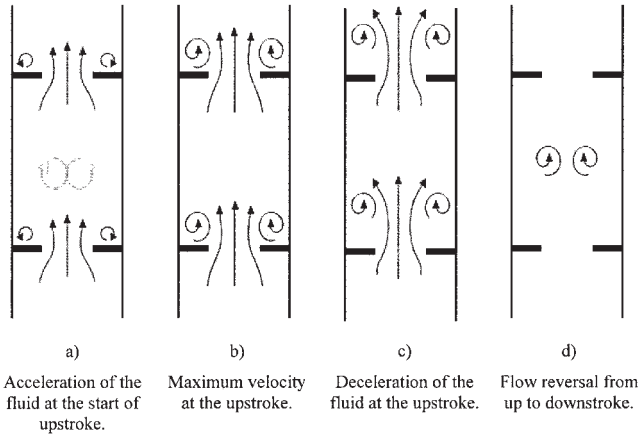

Figure 1. Eddy motion within a baffled column during half a cycle of oscillation.

It is the process of eddy formation and subsequent ejection into the bulk of the cell that is responsible for the intensive mixing achieved in the OBC (Howes and Mackley, 1990; Mackley and Ni, 1991). The chaotic nature of the flow is such that the radial velocity components within the OBC are of the same order of magnitude as the axial components (Ni et al., 1995b). The intensity of mixing can be controlled by varying the oscillatory (amplitude and frequency) and geometrical (baffle spacing and baffle free area) conditions. The oscillatory flow in an OBC is usually described in terms of two- dimensionless groups, the oscillatory Reynolds number ($Re_o = (\omega x_o \rho_L D_C/\mu)$) and the Strouhal number ($St = (D_C/4\pi x_o)$), where D_C is the column diameter (m), ρ_L is the fluid density (kg m^{-3}), μ is the fluid viscosity (kg m^{-1} s^{-1}), ω is the angular frequency ($\omega = 2\pi f$), f is the oscillation frequency (Hz) and x_o is the center-to-peak amplitude of oscillation (m). The OBC is suited for both single and multiphase systems, and excellent performance was reported for suspension of solids (Mackley et al., 1993), dispersion of immiscible liquids (Zhang et al., 1996), and gas-liquid mass transfer (Hewgill et al., 1993; Ni et al., 1995a). The latter studies revealed that substantially enhanced volumetric mass-transfer coefficients can be obtained in the OBC relative to conventional gas-liquid contacting devices, such as bubble columns and stirred tanks. Although experimental results of gas holdup in a reciprocating-plate column fitted with single-orifice baffles (Baird et al., 1996) and some preliminary experimental data of bubble size and gas holdup in an OBC (Oliveira and Ni, 2001) have been published, the physical phenomena controlling the gas-liquid hydrodynamics in an OBC are still poorly understood. In this article, we present a detailed fundamental study on a gas-liquid system, with the aim of understanding the hydrodynamics of the gas-liquid dispersion within the OBC. Emphasis has been placed on establishing a relation between the experimental results and the nature of the flow within an OBC.

Experimental Apparatus

Figure 2 shows the experimental setup and the main components of the OBC, together with the relevant dimensions. The internal diameter and height of the open-top column are 50 mm and 1.5 m, respectively. All experiments were performed in batch mode at atmospheric pressure, room temperature, and tap water was used as the continuous phase. For the purpose of flow visualization, the column was made of transparent extruded Perspex tubing. Square viewing boxes made of Perspex sheeting and filled with water were used to reduce refractive effects caused by wall curvature. The set of 14 polytetrafluorethylene (PTFE) single-orifice baffles, also shown in Figure 2, was designed to fit closely to the column wall. The orifice diameter (D_{bo}) ensured a 23% free cross-sectional area (α).

The fluid oscillator (see, for example, Oliveira and Ni, 2004) was operated sinusoidally, leading to the following function for displacement (x)

$$x = -x_o \cos(\omega t) \quad \text{(m)} \tag{1}$$

where t is time (s). Oscillation frequencies of 0.2 to 10 Hz could be obtained using the speed controller, and center to peak oscillation amplitudes of 1 to 10 mm could be selected by adjusting the off-center (eccentric) position of the connecting rod in the stainless steel coupling wheel. A triggering system was used to allow for the determination of the phase of the oscillation cycle at which each measurement was performed. It consists of a mild steel marker installed in the stainless steel coupling and a hall-effect transistor placed close to the coupling.

Air was continuously fed to the OBC system via a sparger located approximately 40 mm from the base of the column. Two different types of sparger were used: a single-orifice sparger of 1 mm dia. (sparger 1), and a porous borosilicate glass sparger (sparger 2). For the latter sparger, the bubbles are

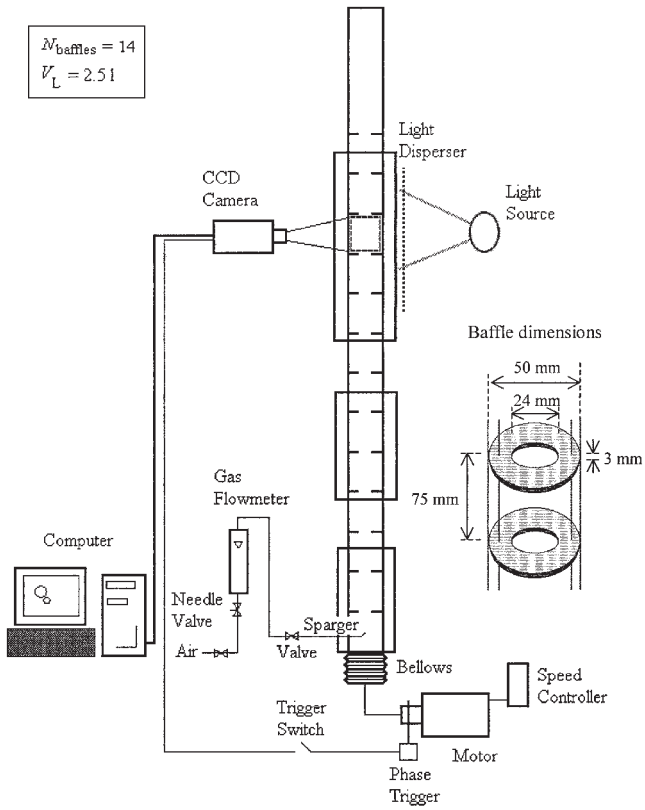

Figure 2. Experimental apparatus (not drawn to scale).

Table 1. Range of Operational Variables Examined in Bubble Size Experiments

Analysis Performed By	x_o (mm)	f (Hz)	Re_o	St	vvm
Software	0	0	0	—	0.05–0.2
Software	2, 4, 8	1–3	624–7489	2.0, 1.0, 0.5	0.05–0.2
Manually	8	4, 5	9985, 12481	0.5	0.05
Manually	4	4–6	4993–7489	1.0	0.05
Manually	4	4, 5	4993, 6241	1.0	0.1

distributed across the entire radius of the column, while, for the former, these are mainly confined to the central core of the column. Aeration rates ranging from 0.05 to 0.3 vvm were used in this work, where vvm is the volume of air per volume of liquid per min. The conversion between the aeration rates expressed in terms of vvm and the superficial gas velocities is given by $U_G = (vvm \times V_L/A_C)$, where A_C stands for the column cross-sectional area (m^2) and V_L for the liquid volume in the column (m^3). Further details of the experimental setup are given elsewhere (Oliveira and Ni, 2004; Oliveira, 2003).

Procedure of Bubble Size Measurement

Measurements of bubble size were carried out using an optical technique. The optical system consisted of a CCD camera (Jai CV-M1) with a 55 mm micro Nikkor lens (minimum *f*-number of 2.8), together with the associated data acquisition units. The camera has a 1,300 by 1,000 CCD pixel array. It was operated at a shutter speed of 3,000 s^{-1} throughout the work, and the depth of field was adjusted to about 2 cm.

Images of bubbles were acquired using the VidPIV 4.0 software package from Optical Flow Systems, Ltd. and directly transferred to a personal computer. Image analysis was performed using both Adobe® Photoshop® and Aequitas - IA (version 1.3) image analysis software (Dynamic Data Links, Ltd.). Measurements of bubble size were performed using the software for the range of operating conditions shown in Table 1. The projected area of each bubble (A_B), determined using the software, was converted to an equivalent diameter (D_{eq}), that is, the diameter of a circle having the same area as the projected area of the bubble, according to Eq. 2

$$D_{eq} = \sqrt{\frac{4A_B}{\pi}} \quad \text{(m)} \tag{2}$$

The normalized bubble-size distribution (BSD) curves were generated by plotting the bubble number fraction vs. D_{eq}. Finally, the mean "volume-to-surface" diameter, termed as the Sauter mean diameter (D_{32}), can be calculated from the experimentally measured values of D_{eq}, by performing a sum over all bubbles

$$D_{32} = \frac{\sum_{j=1}^{N_B} D_{eq_j}^3}{\sum_{j=1}^{N_B} D_{eq_j}^2} \tag{3}$$

where D_{eqj} is the equivalent diameter of bubble *j,* and N_B the total number of bubbles measured. Repeatability and sampling tests in the OBC showed that at least 200 bubbles must be measured in order to guarantee representative BSDs (Oliveira, 2003). In this work, a minimum of 500 bubbles was analyzed for each set of experimental conditions. In general, the data analysis was a very time-consuming process, and the capability of the software is reduced when either the flow rate or the oscillation frequency/amplitude increases, mainly due to bubble overlapping and distortion. The detailed discussions of the image analysis procedure and its limitations are given elsewhere (Oliveira, 2003). In order to overcome the limitations of the software, a few measurements were performed at higher fluid oscillations using a "manual" technique. The technique involved classifying bubbles in a given image into several size ranges, for example, <1 mm, 1-2 mm, 2-3 mm, . . . , >10 mm in dia., using a calibrated scale. Although this method is rather crude, it nevertheless provided an estimation of the mean bubble diameter at high oscillation conditions. Table 1 also lists the conditions at which data analysis was carried out using the manual technique.

Procedure of Gas Holdup Measurement

The volume expansion technique was used to measure the overall gas holdup. This technique involved measuring the level of the multiphase dispersion (H_T) when gas was continuously introduced at a given flow rate, and the corresponding liquid level (H_L) at the top of the column after interrupting the gas flow and allowing the bubbles to escape. The CCD camera was used to record the height of the fluid against a fine scale fixed on the column wall. The triggering system ensured consistency between the phases of the cycle at which the measurements of H_L and H_T were taken. This allowed for accurate and synchronised readings of the fluid levels.

The gas holdup (ε_G) is defined as the volume fraction of the gas phase in the dispersion. It was evaluated from the measured fluid levels by

$$\varepsilon_G = \frac{V_G}{V_L + V_G} = \frac{H_T - H_L}{H_T - N_{\text{baffles}} T_b (1 - \alpha)} \tag{4}$$

which includes a correction to account for the volume of the baffles. In the above equation, V_G is the volume of the gas phase in the column (m^3), T_b is the baffle thickness (m), and $N_{baffles}$ is the total number of baffles in the column. The full range of conditions for which the gas holdup was measured is shown in Table 2.

Table 2. Range of Operational Variables Examined in Gas Holdup Experiments

x_o (mm)	f (Hz)	Re_o	St	vvm
0	0	0	—	0.05–0.2
2	1–6	624–3742	2.0	0.05–0.2
4, 8	1–5	1248–12481	1.0, 0.5	0.05–0.2

Estimation of Power Density

Two models were considered to estimate the power density (P/V) in an OBC: the quasi-steady flow model (Jealous and Johnson, 1955) and the acoustic model (Baird and Stonestreet, 1995). The former was first applied to oscillatory flows by Jealous and Johnson (1955) in a pulsed plate extraction column, and later used in a reciprocating plate column (Hafez and Baird, 1978) and in an OBC (Hewgill et al., 1993; Ni and Mackley, 1993), and can be expressed as

$$(P/V)_{Quasi\text{-}steady} = \frac{2\rho_L N'_{\text{baffles}}}{3\pi C_o^2}\frac{1-\alpha^2}{\alpha^2}x_o^3\omega^3 \tag{5}$$

where C_o is the orifice coefficient (taken as 0.7), and $N_{\text{baffles}}{}'$ the number of baffles per unit length (m^{-1}). The assumption that oscillatory flows are quasi-steady implies that the instantaneous frictional pressure drop in the periodic flow is identical to the pressure drop that would be obtained at a steady velocity of the same magnitude of the instantaneous velocity. In the quasi-steady model, the frictional pressure drop was assumed to be mainly due to the flow through the orifice, neglecting drag forces at the wall. This model has been proven effective for predicting power dissipation rates in an OBC for high-oscillation amplitudes and low frequencies, that is, amplitudes of 5 to 30 mm and frequencies of 0.5 to 2 Hz (Baird and Stonestreet, 1995). For lower amplitudes (1 to 5 mm) and higher frequencies (3 to 14 Hz), the quasi-steady model was found to underestimate the power dissipation (Hafez and Baird, 1978). For those ranges, an alternative acoustic model was developed (Baird and Stonestreet, 1995) by analogy with the acoustic resistance of a single orifice in a thin plate. This new approach considered that the turbulent energy dissipation was localized near the edges of the plates in the same way as in acoustic flows. The acoustic model was based on the work of Panton and Goldman (1976), who showed that at low acoustic intensities the frictional pressure drop at an orifice was related to the kinematic viscosity of the fluid. Baird and Stonestreet (1995) replaced this kinematic viscosity with a much greater eddy kinematic viscosity, based on the assumption that the eddy size in an OBC is much smaller than the tube diameter at high oscillations. The eddy kinematic viscosity was considered to be a function of the oscillation frequency and a mixing length corresponding to the average distance travelled by turbulent eddies. In this case, the power density can be expressed as

$$(P/V)_{Acoustic} = 1.5\,\frac{\rho_L N'_{\text{baffles}}\omega^3 x_o^2 \ell}{\alpha} \tag{6}$$

where λ is the referred mixing length (adopted as 7 mm according to Baird and Stonestreet, 1995). The acoustic model is valid when the amplitude is less than a critical value (Baird and Rama Rao, 1995), which depends on the mixing length and the baffle free area

$$x_{o_{critical}} = \left(\frac{9\pi}{4}\right)\left(\frac{\alpha C_o^2}{1-\alpha^2}\right)\ell \quad \text{(m)} \tag{7}$$

This criterion was employed in this study for the calculation of the power dissipation in the OBC. In brief, the range of power density in the OBC falls into both the quasi-steady and acoustic models depending on the oscillation amplitude and frequency used.

In addition to the external power supplied to the OBC, the power due to the rising gas bubbles should also be considered. This term was originally suggested by Calderbank et al. (1960) and has widely been used in connection with oscillatory flows (Baird and Garstang, 1972; Baird and Rama Rao, 1988; Hewgill et al., 1993). It is given by

$$(P/V)_{Bubbles} = \rho_L g U_G \tag{8}$$

where g is the acceleration due to gravity ($m\ s^{-2}$). Therefore, in gas-liquid systems, the overall time-averaged power density is the sum of two terms, one due to oscillation and the other due to the rising bubbles

$$P/V = (P/V)_{oscillation} + (P/V)_{Bubbles} \tag{9}$$

Results and Discussions of Bubble Size

The application of oscillatory motion to a baffled column induces significant modifications in bubble trajectories, resulting in a complex gas-liquid mixing pattern, which is strongly affected by the amplitude and frequency of oscillation. Figure 3 shows typical bubble images obtained in the OBC with the orifice sparger (sparger 1), at a fixed amplitude, gas-flow rate, and oscillation phase for different frequencies. At low frequencies, large bubbles can be observed in the dispersion and are seen to always move upward. As the frequency increases, these large bubbles breakup and give rise to medium and very small bubbles, which are clearly visible in Figure 3c. These bubbles move downward in certain phases of the oscillation cycle, exploring all the regions of the baffled cells. At very intense

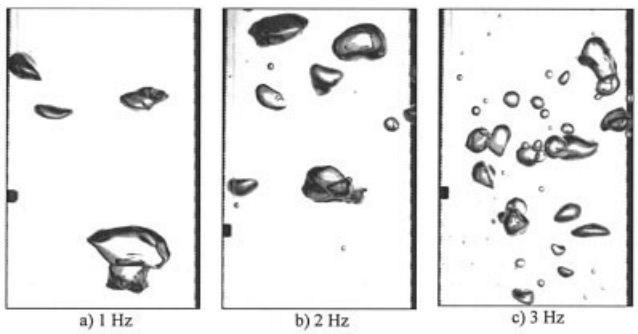

Figure 3. Digital images (≈ 40 mm by 63 mm) of bubbles in the OBC with sparger 1 (x_o = 8 mm, aeration rate =0.1 vvm.

Gas bubbles move upward.). (a) 1 Hz; (b) 2 Hz; (c) 3 Hz.

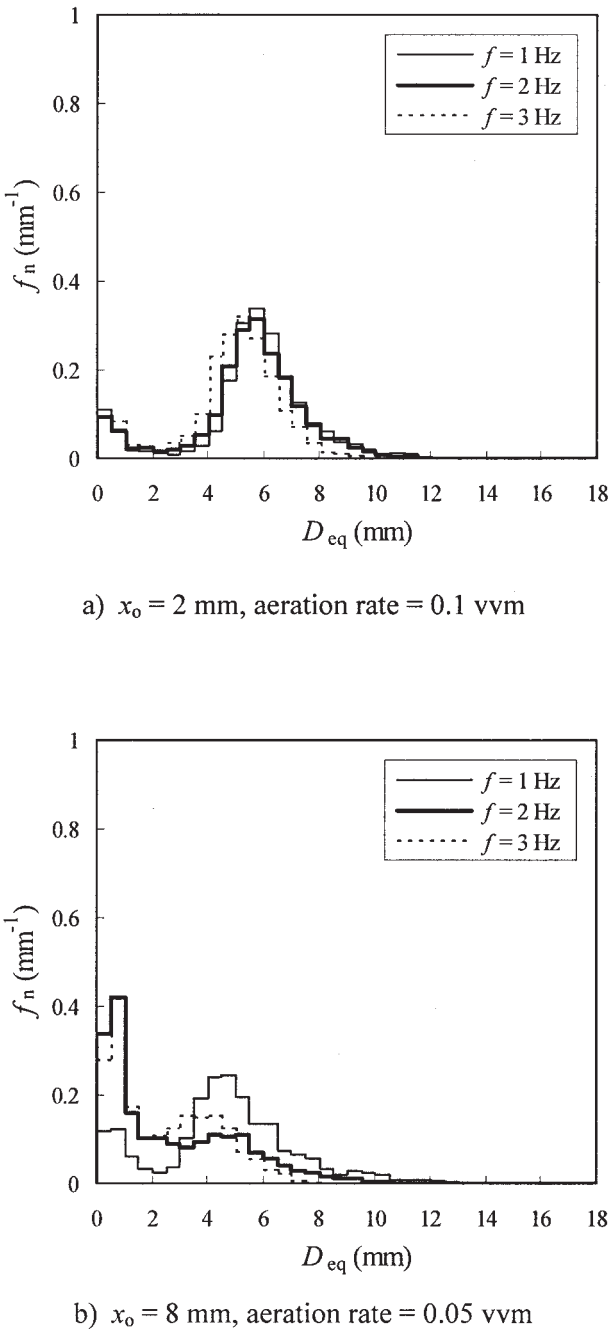

Figure 4. Effect of oscillation frequency on bubble-size distribution in the OBC with sparger 1.

(a) x_o = 2 mm, aeration rate = 0.1 vvm; (b) x_o = 8 mm, aeration rate = 0.05 vvm.

levels of oscillation, rising bubbles are trapped within each cell for a substantial amount of time. The same phenomenon was also observed for the case of single bubbles rising in an OBC (Oliveira et al., 2003a,b).

The effect of oscillation frequency on the bubble-size distribution is shown in Figure 4a for a low amplitude of 2 mm, and in Figure 4b for a higher amplitude of 8 mm. In the first case, the increase of the oscillation frequency has little effect on the BSD, as the curves exhibit similar characteristics in both shape and diameter range. When the higher amplitude was used (Figure 4b), the increase in the oscillation frequency narrowed the BSD and shifted the BSD to lower equivalent diameters. At these high intensities of oscillation, bubble breakage increases, since bubbles above a certain critical size become unstable.

Similar effects of oscillation amplitude on the BSD are shown in Figure 5a for a low frequency of 1 Hz, and in Figure 5b for a higher frequency of 3 Hz. As in Figure 4, all bimodal distributions shifted toward lower equivalent bubble diameters

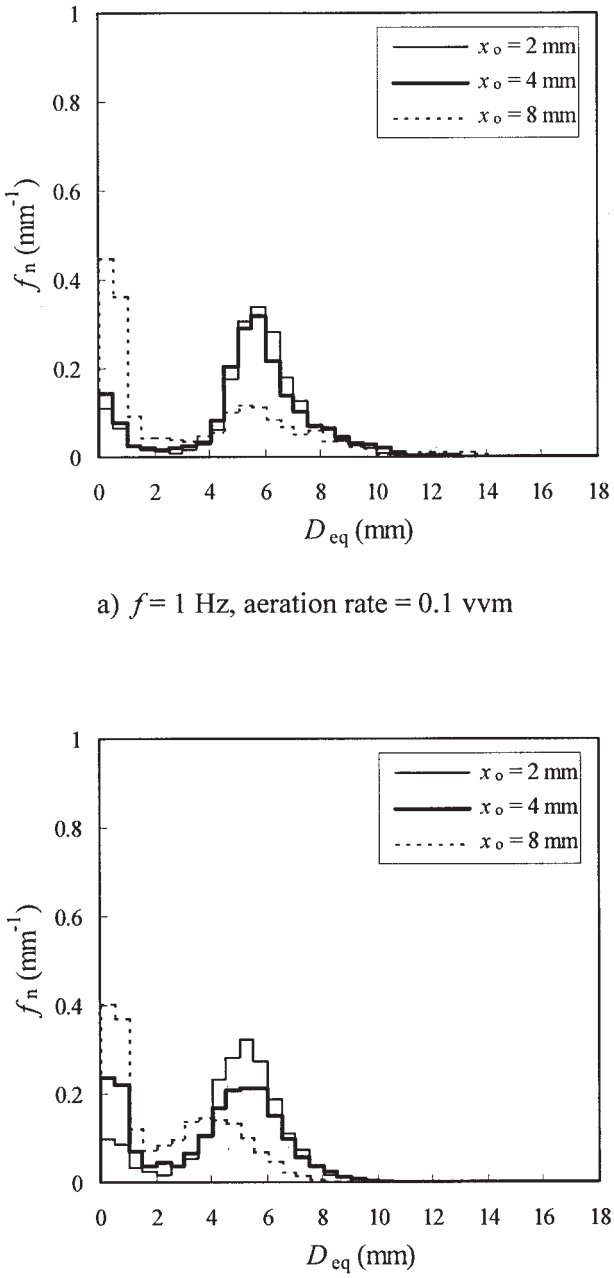

Figure 5. Effect of oscillation amplitude on bubble-size distribution in the OBC with sparger 1.

(a) f = 1 Hz, aeration rate = 0.1 vvm; (b) f = 3 Hz, aeration rate = 0.1 vvm.

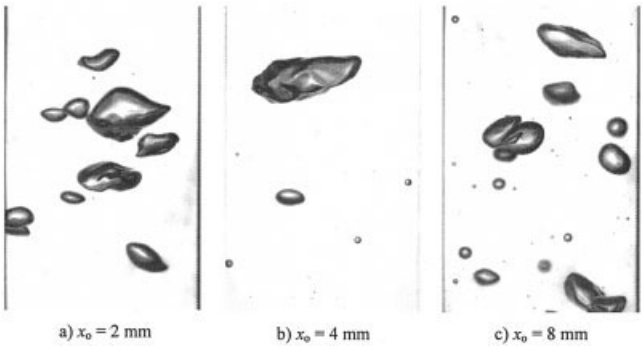

Figure 6. Digital images (≈ 40 mm by 63 mm) of bubbles in the OBC with sparger 2 (f = 2 Hz, aeration rate = 0.05 vvm).

Gas bubbles move upward. (a) x_o = 2 mm; (b) x_o = 4 mm; (c) x_o = 8 mm.

as the oscillation amplitude increased. Increasing the oscillation amplitude promotes bubble breakage, thus growing the percentage of smaller bubbles (< 2 mm) at the expense of larger ones (> 4 mm). This effect is more significant at higher frequencies.

Figure 6 shows typical bubble images obtained in the OBC with sparger 2 for different oscillation amplitudes, taken at the same location and phase as those shown in Figure 3. For the porous glass sparger, the presence of large bubbles is seen at low oscillation levels, but at higher oscillations, evidence of bubble breakage can also be observed. The effect of oscillation frequency on BSD for sparger 2 is given in Figure 7a at a fixed amplitude of 4 mm and aeration rate of 0.05 vvm, and the effect of oscillation amplitude on BSD in Figure 7b at a fixed frequency of 2 Hz and aeration rate of 0.05 vvm. Although the effect of fluid oscillation on the BSD for sparger 2 is qualitatively similar to that for sparger 1, the characteristics of the BSDs are considerably different. Noticeably, there is a higher number of large bubbles present for sparger 2, manifested by a long tail in the distribution at large diameters. At the same time, there is also a higher proportion of very small bubbles. As in the case of sparger 1, an increase in either frequency or amplitude of fluid oscillation brings about substantial breakage of large bubbles, evidenced by a decrease in the tail of the distribution, and by an increase in the percentage of small bubbles.

Figure 8 illustrates the effect of oscillation frequency and amplitude, as well as aeration rate, on the Sauter mean diameter. Note that there are only two aeration rates used at the highest oscillation amplitude (Figure 8c), due to the difficulty in obtaining good enough images of bubbles at these conditions. It can be seen that as the oscillation frequency increases, the Sauter mean diameter decreases. At low amplitudes (Figure 8a), the decrease is gentle in the range of frequencies applied, but for higher values of amplitude, the decrease becomes stronger, and occurs at lower frequencies for higher aeration rates. This is due to the fact that, at higher aeration rates, bubbles are larger and, therefore, become unstable (and prone to breakage) at lower oscillation levels. It can also be seen that at low oscillations the D_{32} increases with the aeration rate. This is expected, as there is a higher density of bubbles in the column at high aeration rates, and, therefore, an increased tendency for bubble coalescence. However, this effect is hindered as the intensity of the oscillatory motion in the column becomes larger, and the dependence of D_{32} on the aeration rate gradually disappears at high levels of oscillations (Figure 8b and c at frequencies above 3 Hz). Above a certain critical oscillation level, D_{32} decreases strongly with both f and x_o.

Figure 9 presents a direct comparison between the Sauter mean diameters obtained in the OBC for both spargers, as a

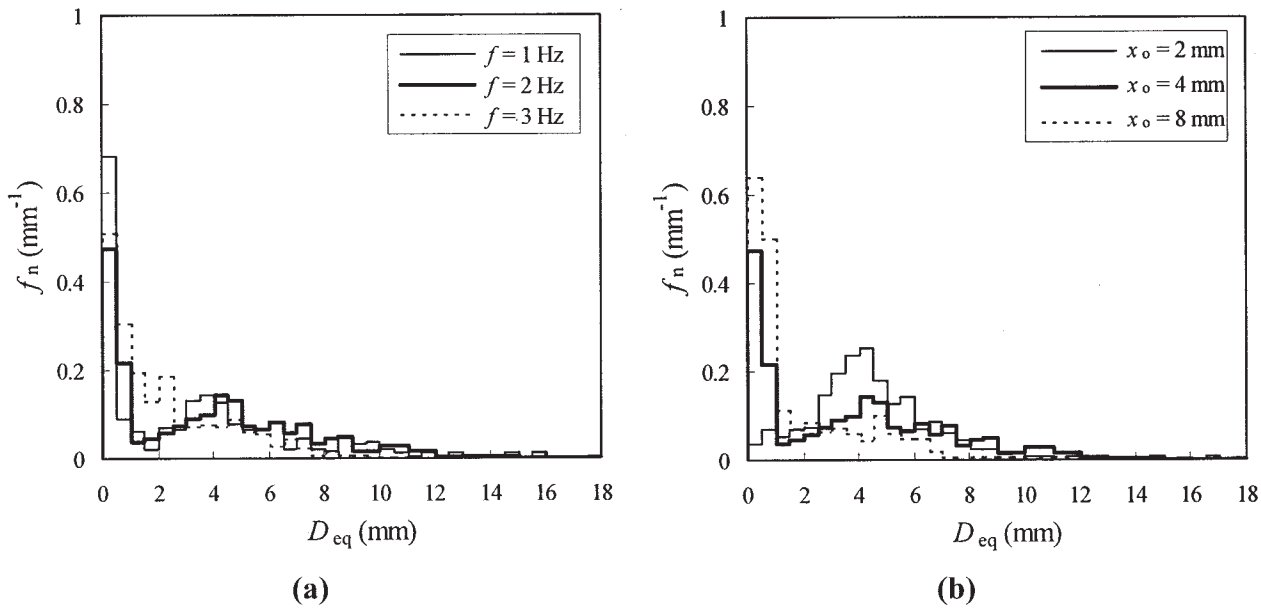

Figure 7. (a) Effect of oscillation frequency on bubble-size distribution in the OBC with sparger 2 (x_o = 4 mm, aeration rate = 0.05 vvm); (b) effect of oscillation amplitude on bubble-size distribution in the OBC with sparger 2 (f = 2 Hz, aeration rate = 0.05 vvm).

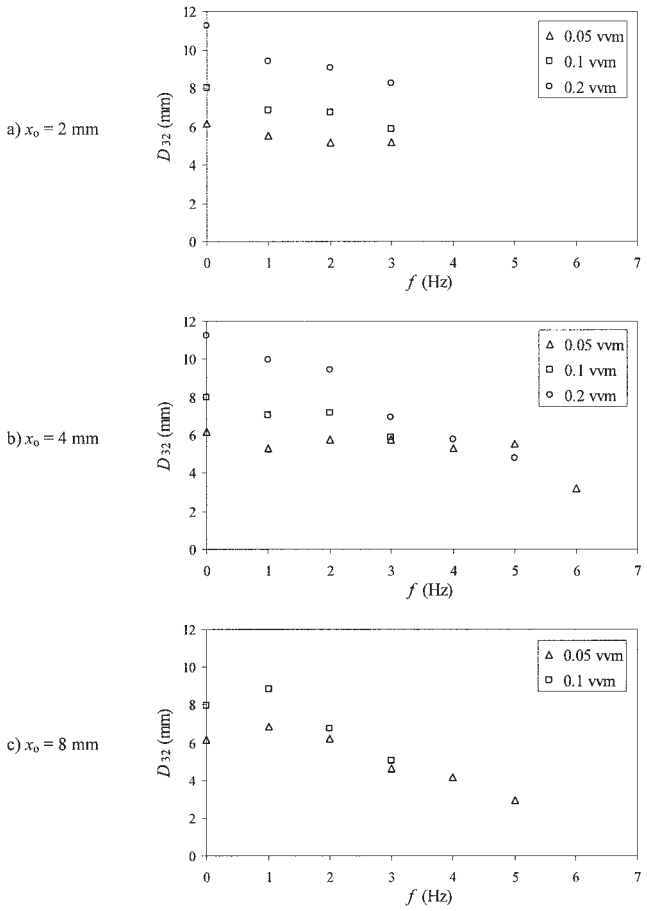

Figure 8. Effect of oscillation frequency on Sauter mean diameter in the OBC with sparger 1.

(a) x_o = 2 mm; (b) x_o = 4 mm; (c) x_o = 8 mm.

function of oscillation frequency and amplitude. We see that at low levels of oscillation, the values of D_{32} for sparger 2 lie above those for sparger 1. At the first sight, this might seem surprising, since the former sparger produces smaller bubbles than the latter in a bubble column. However, the presence of baffles strongly promotes bubble coalescence for sparger 2, since in this case the bubbles are distributed along the entire radius of the column and not confined to a more central path (Oliveira, 2003). The most significant point to note in Figure 9, however, is that the differences in D_{32} between the two spargers become insignificant at high oscillation levels.

From the analysis of Figures 8 and 9, it is clear that there are two distinct operating regions with respect to the bubble sizes in an OBC. At low oscillation levels, the bubble sizes are mainly influenced by variables, such as the gas flow rate and the sparger type. Above a critical oscillation level, see for example, those for frequencies of 2 Hz and earlier in Figure 8c, the amplitude and frequency of oscillation are the main parameters controlling bubble breakage and, hence, the value of D_{32}. This indicates that different physical processes may dominate in the two regions. In this article, we are mainly interested in analyzing the phenomena at high oscillation levels, since this is the region of practical interest for mass-transfer applications of the OBC (Oliveira and Ni, 2004).

Risso (2000) recently published a detailed review of the mechanisms of bubble and drop breakage in different types of two-phase flows. Depending on the physical properties of the fluids and on the nature of the flow, breakage may be due to deformations caused by viscous or inertial effects. Breakage criteria are usually expressed in terms of the ratio of the stress causing the deformation (τ) to the surface tension stress (σ/D_B) contributing to the integrity of the bubble. Viscous effects are predominant only in the limit of low-Reynolds numbers, and are, thus, of little importance to this study. When deformation is driven by inertia, breakage criteria are expressed in terms of a generalized Weber number (Hinze, 1955)

$$We = \frac{\tau D_B}{\sigma} = \frac{\rho_L u_R^2 D_B}{\sigma} \tag{10}$$

where u_R is a characteristic velocity of the bubble relative to the liquid (m s^{-1}), and D_B the bubble diameter (m). The inertial stress can be due to a number of causes, such as the mean drift due to buoyancy, the mean strain rate and turbulent velocity fluctuations (Risso, 2000). Depending on the dominant mechanism, the characteristic velocity will assume different forms. In most practical situations, however, all of the above mechanisms are present, and the analysis of bubble breakage becomes a troublesome process. In order to attempt a quantitative de-

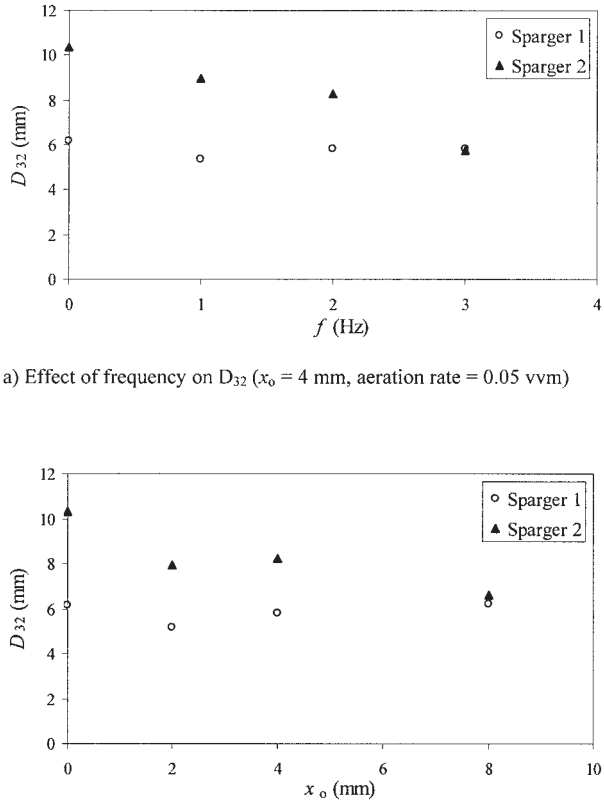

a) Effect of frequency on D_{32} (x_o = 4 mm, aeration rate = 0.05 vvm)

b) Effect of amplitude on D_{32} (f = 2 Hz, aeration rate = 0.05 vvm)

Figure 9. Sauter mean diameter in the OBC with two different spargers.

(a) Effect of frequency on D_{32} (x_o = 4 mm, aeration rate = 0.05 vvm); (b) Effect of amplitude on D_{32} (f = 2 Hz, aeration rate = 0.05 vvm).

scription of the experimental D_{32} results obtained in the OBC, the dominant mechanism for bubble breakage must be identified. In the high oscillation region, the bubble motion is mainly controlled by the oscillatory motion of the fluid (see gas holdup discussion in next section), so it is reasonable to assume that buoyancy effects are of secondary importance. Thus, bubble breakage in the OBC in the high oscillation region is most likely dominated by either the large relative velocity gradients of the main flow or by turbulent velocity fluctuations. For the time being, we will assume that the latter is the dominant mechanism. This assumption will be analyzed later in this section.

On the basis of this hypothesis, a model proposed by Hinze (1955) and Kolmogoroff (1949), based on Kolmogoroff's "isotropic turbulence theory" (Kolmogoroff, 1941), was applied to the experimental results of the Sauter mean diameter in the OBC at high oscillations. The isotropic turbulence theory describes turbulent flow as consisting of a hierarchy of eddies of different magnitudes, and the kinetic energy of the flow is transferred from the primary eddies down to the microscale viscous ones. Kolmogoroff postulated that the small viscous eddies are statistically independent of the main flow, and are, thus, locally homogeneous and isotropic. This is true even if the main turbulent flow is not, on the whole, isotropic (Kolmogoroff, 1941). To confirm the existence of local isotropy in the OBC at high oscillation levels, the kinetic energy spectrum of the flow has to be examined. Unfortunately, to date no such study has been performed in an OBC. As mentioned previously, Roberts and Mackley (1996) have shown that the flow in an OBC loses its symmetry and becomes chaotic at values of Re_o above the order of 200. Recently, Ni et al. (2003b) have presented the determination of the turbulent integral length scale in an OBC, but this work was also restricted to relatively low oscillation levels ($Re_o < 2{,}500$). To complicate the matter, the presence of the bubbles themselves is likely to alter the characteristics of the flow. All things considered, it is unlikely that the flow in the OBC would be completely turbulent and isotropic. Nevertheless, we believe that at sufficiently high oscillatory Reynolds numbers, there is significantly high unsteadiness/chaotic/turbulence in the system to provide a size range much smaller than the dominant eddy size. It is this condition that is dominated by turbulence in the OBC. The turbulence at this scale will only depend on the power dissipation per unit mass of fluid (ε) and on the kinematic viscosity (ν). By dimensional reasoning, Kolmogoroff derived the following expression for the length scale (η) of the viscous eddies

$$\eta = \left(\frac{\nu^3}{\varepsilon}\right)^{1/4} \quad \text{(m)} \tag{11}$$

For local isotropy to exist, η must be small compared to the characteristic length scale (L) of the main flow. The value of η was calculated for the range of oscillations considered, given that ($P/V = \varepsilon\rho_L$), and was found to be at most of 0.07 mm. If we consider the length scale of the main flow to be of the order of the column diameter (50 mm), we see that the above condition is rightfully satisfied.

A further hypothesis of the isotropic turbulence theory is the existence, for large Reynolds numbers, of a so-called "inertial subrange" at length scales (l) above the viscous dissipation range. In the inertial subrange, viscous dissipation is unimportant, and, thus, the turbulence is independent of ν and solely determined by ε. Therefore, the following equation applies (Batchelor, 1953)

$$u = C_1(\varepsilon l)^{1/3} \quad (\text{m s}^{-1}) \tag{12}$$

where u is the mean square turbulent velocity fluctuation difference over a distance l and C_1 is approximately $2^{1/2}$ (Batchelor, 1953). In order for an inertial subrange to exist, l must be small compared to L, but much larger than η. Also, according to Shinnar (1961), the following condition should be satisfied

$$(Lu/\nu)^{3/8} > 1 \tag{13}$$

In order to apply the above theory to the modeling of bubble size, Hinze (1955) assumed that, in a locally isotropic turbulent flow, bubble breakage is caused by deformations of the surface induced by the eddies in the inertial subrange. This is true when the bubble diameter (D_B) is of the same scale as these eddies. Larger eddies will only transport bubbles, while smaller eddies have insufficient energy to cause bubbles to breakup. If we compare the values of the Sauter mean diameter at high oscillations (Figure 8) with the length scale of the main flow and η, we see that $L > D_{32} \gg \eta$ is true above the critical oscillation level. Furthermore, Eq. 13 is satisfied for those conditions (the expression on the lefthand side is always larger than 25). This means that, if the turbulence mentioned previously is assumed to be isotropic, the conditions for the existence of an inertial subrange at the length scale of the bubble diameter are fulfilled.

In Hinze's model, based on a static force balance, breakage occurs when *We* exceeds a certain critical value. As discussed by Risso and Fabre (1998), this critical value is probably not universal, since it is likely to depend on the bubble residence time. Hinze's model essentially assumes that the bubble resides in the fluid for long enough time to experience all possible turbulent fluctuations. Risso and Fabre (1998) have proposed a correction to the critical Weber number (termed the "efficiency factor", which depends on the bubble residence time) to account for situations in which the residence time of the bubble is not sufficient to satisfy the above assumption. In the OBC at high oscillation levels, considering a large enough residence time is a considerably reasonable approximation, since the bubbles are trapped in each baffled cell for a significant period of time. Although direct measurement of the residence time in the OBC is precluded at the present conditions, single bubble studies (Oliveira et al., 2003a) suggest that the bubble residence time immediately above the critical oscillation level is about 10 s, and that it is not very sensitive to the bubble diameter in the size ranges studied here. Nevertheless, the critical *We* will not be strictly the same for all the bubbles in the flow field, and, thus, should be interpreted as an average value (Hinze, 1955).

The critical Weber number is calculated by substituting Eq. 12 for the characteristic velocity in Eq.10. Taking $l = D_B$, the scaling law for the bubble diameter would be

$$D_B \propto \frac{\sigma^{3/5}}{\rho_L^{3/5}\varepsilon^{2/5}} \quad \text{(m)} \tag{14}$$

Equation 14 is a general correlation for estimating the maximum bubble size that is stable against breakage by turbulent forces. In terms of experimental measurements, the maximum stable bubble size may be approximated by D_{95}, which is the 95th percentile of the bubble-size distribution. In most practical cases, D_{32} is found to be proportional to D_{95} (for example, Baird and Lane, 1973; Parthasarathy and Ahmed, 1996). From the results of the BSDs obtained from this work, it was observed that

$$\frac{D_{32}}{D_{95}} = 0.826 \pm 0.021 \tag{15}$$

within a 95% confidence level. This means that Eq. 14 can be used to predict the Sauter mean diameter in the OBC for operating conditions under which the bubble size is determined by the breakage mechanism. In terms of power density, this equation becomes

$$D_{32} = k \frac{\sigma^{3/5}}{\rho_L^{1/5}(P/V)^{2/5}} \tag{16}$$

where k is a dimensionless constant. Equation 16 has been used to predict bubble diameters in several different types of gas-liquid contactors. Applications of the isotropic turbulence theory to stirred tanks run into difficulties, largely due to the nonhomogeneous distribution of the energy dissipation, which is usually much higher near the impeller than in the bulk of the tank (Schügerl, 1982; Tsouris and Tavlarides, 1994). Modified versions of the earlier equation have been reasonably successful (for example, Kawase and Moo-Young, 1990; Calderbank, 1958; Bhavaraju et al., 1978). The model has also been applied to turbulent pipe flows (for example, Karabelas, 1978; Hesketh et al., 1987), leading to several expressions for the critical *We*. Zakrzewski et al. (1981) showed that the mechanism of energy dissipation in bubble columns was very similar to that proposed in the isotropic theory. Kolmogoroff's theory was also successfully applied to predict droplet sizes in a reciprocating plate column (Baird and Lane, 1973), and in an OBC (Ni et al., 1998).

The isotropic turbulence theory can also be extended to a situation in which the stable bubble size is determined by coalescence rather than breakage (Thomas, 1981; Shinnar, 1961; Sprow, 1967). In such a case, a different functional dependence of D_{32} with the power density is predicted

$$D_{32} \propto (P/V)^{-1/4} \tag{17}$$

It is expected that in a real situation, where both coalescence and breakage are significant and the stable bubble size is dictated by an equilibrium between the two phenomena (Shinnar, 1961), the exponent of the power density will lie somewhere between the values predicted by Eqs 16 and 17. In order to test the validity of the earlier models, the experimental D_{32} data can be fitted to a general expression of the form

$$D_{32} = k'(P/V)^p \tag{18}$$

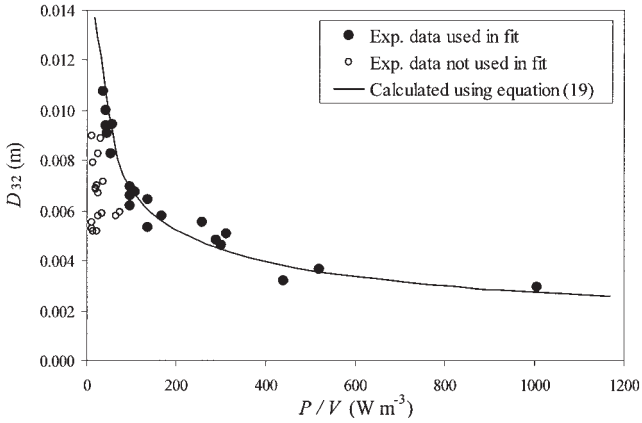

Figure 10. Effect of power density on Sauter mean diameter (sparger 1 and 2).

The open circles correspond to D_{32} data in the range of low oscillations.

with k' and p as fitting parameters. Using Eqs. 5–9 to estimate P/V in the OBC, the experimental D_{32} data were fitted to Eq. 18 yielding a value of -0.389 ($\pm$ 0.045) for the exponent index p. This exponent index is very close (within statistical error) to the prediction of 2/5, based on the turbulent breakage mechanism, suggesting that the stable bubble size in the OBC at high oscillation levels is dictated by bubble breakage brought about by the chaotic nature of the fluid flow. In consequence, the experimental D_{32} data were correlated following the format of Eq. 16 with k as a sole fitting parameter, the best-fit is

$$D_{32} = 0.84 \frac{\sigma^{3/5}}{\rho_L^{1/5}(P/V)^{2/5}} \tag{19}$$

Note that both ρ_L and σ are kept constant in this work, and, thus, the Sauter mean diameter is solely a function of the power density. Figure 10 shows D_{32} as a function of P/V. As discussed previously, the data at oscillations below the critical level (open circles in Figure 10) were not included in the fitting procedure, since in this region the bubble size is certainly not controlled by the interaction of bubbles with eddies of the inertial subrange. In this operating region, other mechanisms of bubble breakage may be predominant, and bubble coalescence plays an important part. However, in the high oscillation region (filled circles in Figure 10), the agreement between the experimental measurements and the correlation is very reasonable.

From Eqs. 10, 12, 15, and 19, the calculated value for the critical Weber number in the OBC is 2.06, which is below the value of 5 given by Risso and Fabre (1998) when turbulence is the single cause of breakage. However, an attempt to describe the experimental results considering the mean strain rate to be the dominant mechanism, that is, using the maximum relative velocity between the bubble and the fluid as the characteristic velocity in Eq. 10, was unsuccessful. These considerations, allied to the robustness of the scaling law given by Eq. 19 in the OBC, suggest that the dominant mechanism is bubble breakage by turbulent fluctuations. However, this is likely not to be the only cause of deformations, and thus the value of *We* calculated here is a cumulative parameter that also includes the contribu-

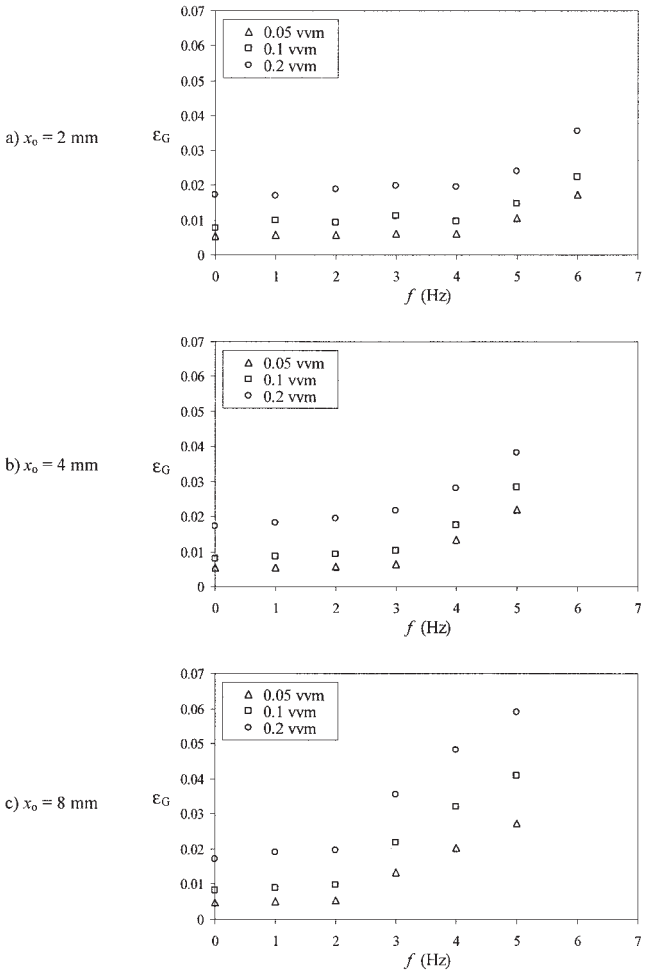

Figure 11. Gas holdup as a function of frequency in the OBC with sparger 1.

(a) x_o = 2 mm; (b) x_o = 4 mm; (c) x_o = 8 mm.

tions of other breakage mechanisms, such as breakage by large-scale velocity gradients.

Results and Discussions of Gas Holdup

The measurements of gas holdup as a function of oscillation frequency in the OBC with sparger 1 are plotted in Figure 11 for different amplitudes and aeration rates. Two patterns can be distinguished: at low fluid oscillation, the changes in holdup are very small, but above a certain frequency that varies with the oscillation amplitude, the gas holdup shows a significant increase. Similar conclusions can be drawn about the effect of amplitude on gas holdup. This pattern is in qualitative agreement with the experimental results of Baird et al. (1996). The increased gas holdup is a combination of two factors, the decrease in bubble sizes and increase in residence time of the gas phase. In terms of the latter, Figure 12 shows images of bubble trajectory at two different frequencies of oscillation. These images were obtained using the CCD camera with a long exposure time. At a low frequency (Figure 12a), the bubbles are seen to rise swiftly from one baffled cell to another, predominantly through the center of the column. At a high frequency, however, the bubbles start to move downward in some phases of the oscillation cycle, and pass through all regions of the baffled cell. The vortical path that the bubbles follow after entering the baffled cell can clearly be viewed in Figure 12b. Bubbles remain trapped in these large-scale vortices for significantly long periods of time. This "washing-machine" effect leads to much higher residence times and, therefore, higher holdups in the OBC.

The effect of decreasing bubble size on gas holdup is not as straightforward as mentioned earlier. On the one hand, lower average rising velocities and higher holdups are expected due to this reduction in bubble diameter. On the other hand, the bubbles that have the most significant impact on gas holdup are those with diameters around D_{32}. In this range, the rise velocity of bubbles is almost independent of their diameter (Clift et al., 1978). This means that the overall effect of the decrease in D_{32} on the gas holdup is relatively small. In summary, the primary cause for an increase in the gas holdup at high oscillations is the change in the trajectories of bubbles, rather than the decrease in bubble size. This is in agreement with the interpretation of Baird et al. (1996).

Another feature showing in Figure 11 is that the higher the aeration rates, the higher the gas holdups. This is expected. The effect of different spargers on holdup is given in Figure 13 where we see that the gas holdups are in fact independent of the sparger types.

A widely used model for predicting gas holdup in bubble columns is based on the concept of slip velocity, discussed by Godfrey and Slater (1991), which, for a batch column, means that

$$u_S = \frac{U_G}{\varepsilon_G} \quad (\mathrm{m\ s^{-1}}) \tag{20}$$

where u_S is the slip velocity of the gas phase relative to the liquid. In bubble columns, the characteristic velocity of the gas phase can be approximated by the average terminal velocity. In an OBC, however, a time-averaged value over all the bubbles in the dispersion should be used in Eq. 20, since the instanta-

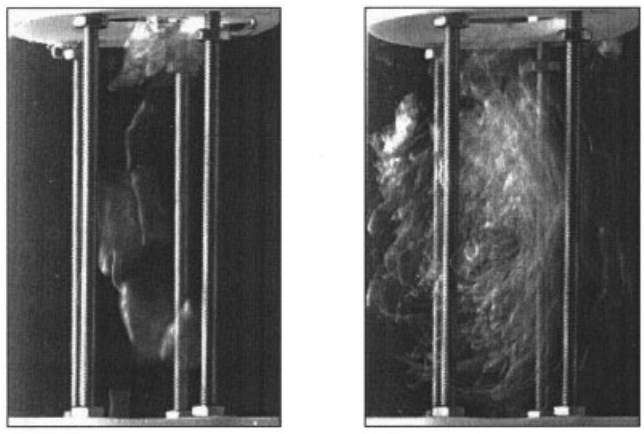

Figure 12. Bubble trajectory (x_o = 4 mm, aeration rate = 0.1 vvm).

(a) f = 1 Hz; (b) f = 6 Hz.

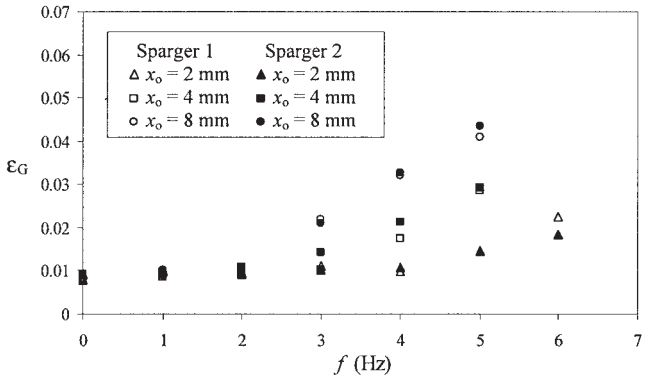

a) aeration rate = 0.1 vvm

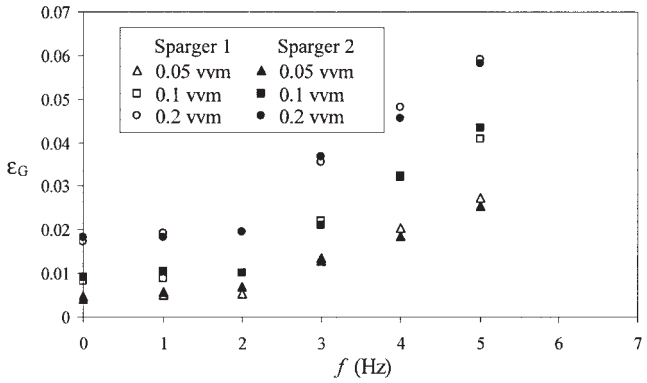

b) x_o = 8 mm

Figure 13. Gas holdup as a function of frequency in the OBC with two different spargers.

(a) aeration rate = 0.1 vvm; b) x_o = 8 mm.

neous velocity of a single bubble oscillates around a certain time-averaged velocity ($\overline{U_B}$) (Oliveira, 2003). Therefore, the holdup can be expressed as

$$\varepsilon_G = \frac{U_G}{\langle U_B \rangle} \tag{21}$$

where the angular brackets denote an average over all bubbles in the dispersion. The values of were estimated using a model based on a simplified balance of forces acting on a single bubble (see Appendix). The resulting equation for the instantaneous velocity of a single bubble of diameter larger than 1.3 mm is

$$\frac{dU_B(t)}{dt} = \frac{g}{a_m} - \frac{3}{4a_m D_B\left(0.378 + \frac{1.605\sigma}{\rho_L g D_B^2}\right)} U_B(t)|U_B(t)| + \frac{3x_o\omega}{2a_m C_o \alpha D_B\left(0.378 + \frac{1.605\sigma}{\rho_L g D_B^2}\right)} \sin(\omega t) U_B(t) + \frac{x_o\omega^2}{C_o\alpha} \times \left(1 + \frac{1}{a_m}\right)\cos(\omega t) - \frac{3x_o^2\omega^2}{4a_m C_o^2\alpha^2 D_B\left(0.378 + \frac{1.605\sigma}{\rho_L g D_B^2}\right)} [\sin(\omega t)]^2 \tag{22}$$

where a_m is the added mass coefficient (taken as 0.5). Equation 22 is a Riccati equation and cannot be solved analytically unless a particular solution is known; however, a numerical solution can be obtained. A computer code to solve the above equation was written in FORTRAN 90 using the NAG library D02EBF. The calculations have shown that fluid oscillation caused the instantaneous bubble velocity to fluctuate around an average value, with the amplitude of these fluctuations increasing with both f and x_o. The calculated time-averaged velocity was seen to decrease as the fluid oscillation increases. It should be noted that the time-averaged bubble velocity used in Eq. 21 is that of an isolated bubble, which is not necessarily the same as the velocity of a bubble in a dispersion, due to interactions with other bubbles.

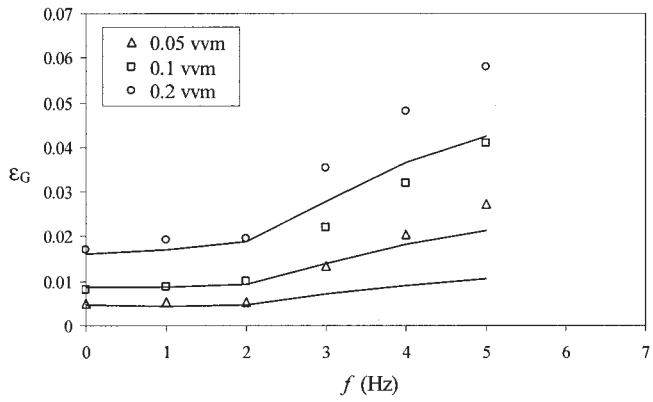

(a)

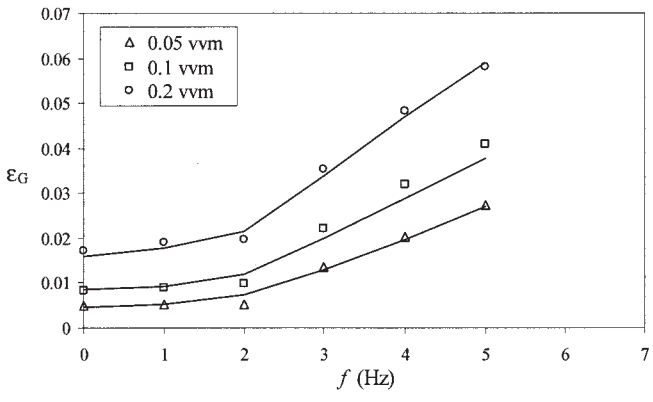

(b)

Figure 14. (a) Experimental gas holdup (symbols) in the OBC with those calculated using Eq. 21 (solid lines) (x_o = 8 mm with sparger 1); (b) experimental gas holdup (symbols) in the OBC with those calculated using Eq. 28 (solid lines) (x_o = 8 mm with sparger 1).

Figure 14a shows a comparison between the experimental gas holdups and those calculated from Eq. 21. The data shown here were obtained in the OBC with sparger 1 at $x_o = 8$ mm and three different aeration rates. In general, the solid lines generated using Eq. 21 match well with the experimental data at low oscillation frequencies, and also accurately describe the points at which the gas holdups start to rise. This is remarkable, considering that the model described earlier is purely theoretical and requires no fitting parameters. However, for higher oscillations the theoretical predictions seriously underestimate the increase in the holdup with the oscillation frequency, probably due to the fact that the force balance for the calculation of the average bubble velocity considered only the forces in the axial direction and neglected the effect of lateral bubble motion on the gas holdup (Oliveira, 2003). It is, therefore, natural to expect that a correction is needed to account for the retention of bubbles by turbulent vortices (shown in Figure 12b). In fact, the phenomenon of particle and bubble suspension in vortical flow fields has been recognized for some time (Tooby et al., 1977; Fung, 1993). The ability of vortices to entrain bubbles is controlled by two-dimensionless parameters (see Sene et al., 1994; Magnaudet and Eames, 2000)

$$\Gamma = \frac{\Omega r_v}{U_T} \tag{23}$$

$$\Pi = \frac{\Omega^2 r_v}{g} \tag{24}$$

where Ω is the angular velocity of the vortex [= ½ ζ] (s^{-1}), ζ the vorticity (s^{-1}), U_T the bubble terminal velocity (m s^{-1}), and r_v the vortex radius (m). Γ is the so-called "trapping parameter", measuring the ratio between fluid velocity at the vortex "rim" and bubble terminal velocity in a stagnant fluid. Π is the ratio between the centripetal force, pulling the bubble toward the vortex core, and the buoyancy force, which tends to drive it past the vortex. High values of the dimensionless number Π mean that it is more difficult for bubbles to escape the vortex, once they are trapped (Sene et al., 1994). It is reasonable to deduce that the residence time of the bubbles in the vortex would depend on Π. A relationship between this parameter and the operating conditions in the OBC can be established as follows. The localized vorticity was calculated using Eq. 25

$$\zeta(x, y) = \frac{\partial \mathbf{u}_{L_y}}{\partial x} - \frac{\partial \mathbf{u}_{L_x}}{\partial y} \tag{25}$$

where $\mathbf{u}_L$ denotes the local fluid velocity vectors, which are directly measured in an OBC of similar geometric characteristics using digital particle image velocimetry (DPIV) (Fitch, 2003), and x and y refer to the cartesian co-ordinates. Using this approach, it is possible to determine the maximum vorticity in the vortex core (which occurs at a distance r_v from the center), for a series of oscillation amplitudes and frequencies. The results are shown in Figure 15, from which it can be seen that the maximum vorticity is directly proportional to the oscillation frequency and independent of the amplitude.

A further conclusion that was drawn from the fluid flow maps is that the size of the vortices depends on the oscillation amplitude and is practically independent of frequency (Fitch, 2003). On the basis of this, Π can be re-written as

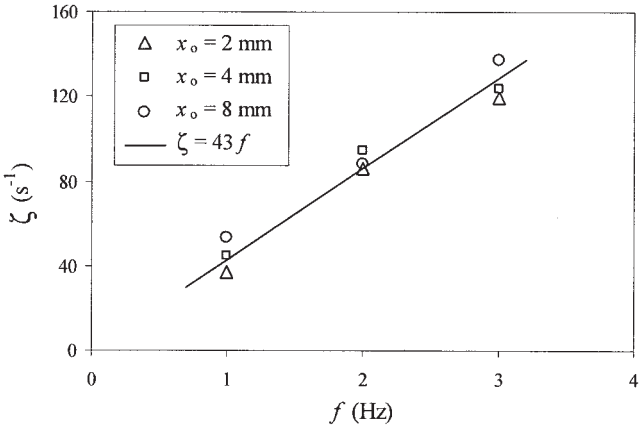

Figure 15. Effect of oscillation on maximum vorticity.

$$\Pi = k \frac{\omega^2 x_o}{g} \tag{26}$$

where k is a dimensionless constant. Considering the effect of the constriction imposed by the baffles, and assuming that the time that the bubbles are trapped in the vortices is proportional to Π, an appropriate expression for the gas holdup can be established as

$$\varepsilon_G = \frac{U_G}{\langle \overline{U_B} \rangle} + k \frac{x_o \omega^2}{C_o \alpha g} \tag{27}$$

The above equation was fitted to the experimental holdup data and a value of $k = 0.0033 \pm 0.00024$ was obtained, and, thus

$$\varepsilon_G = \frac{U_G}{\langle \overline{U_B} \rangle} + 0.0033 \frac{x_o \omega^2}{C_o \alpha g} \tag{28}$$

Figure 14b compares the experimental data with the predictions of Eq. 28, and a much better agreement is achieved for all oscillation levels. The average relative error of the fit is ±9% (Figure 16).

Conclusions

Detailed experimental results concerning the characteristics of a gas-liquid system in an OBC have been reported. At low levels of oscillation, the characteristics of the dispersion depend on the type of sparger and the aeration rate, similarly to that in a bubble column, and the oscillation has little effect. A critical operation condition exists, beyond which the influence of oscillation on both bubble size and gas holdup becomes significant, and the dependence of other variables is considerably reduced.

Analysis of the experimental results, together with flow visualization, enabled the gas-liquid parameters to be described in terms of the flow patterns. The oscillatory flow in the

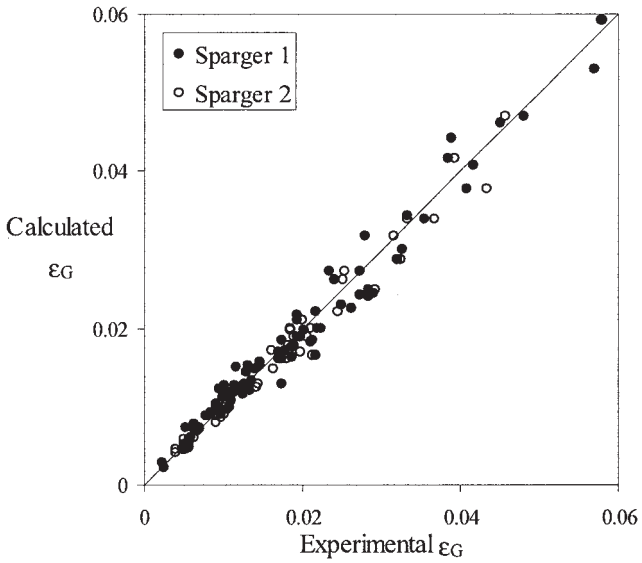

Figure 16. Experimental and calculated gas holdup using Eq. 28.

The solid line represents $y = x$.

presence of baffles induces the formation of eddies within the baffled cells, which are responsible for the good mixing achieved in the OBC. At sufficiently high levels of oscillation, the gas-liquid hydrodynamics are determined by the interactions of bubbles with the turbulent flow structures. Large-scale vortices, which induce a recirculating pattern in each baffled cell, are able to retain the bubbles for long periods of time. This, in turn, leads to the observed increase in the gas holdup. Interaction of the bubbles with eddies of intermediate length scale (of the order of the bubble diameter) are the main cause of breakage, leading to the observed decrease in the Sauter mean diameter. This phenomenon was successfully modeled by applying the isotropic turbulence theory.

This article constitutes a first attempt at gaining a theoretical understanding of the physical phenomena within a gas-liquid oscillatory baffled column. Further studies are necessary in order to validate and improve the approach presented here. In particular, systematic studies of spatio-temporal spectra of the flow field in an OBC at high oscillation would provide insight into the precise nature of the flow and the extent of turbulence. A particular aspect that should be investigated further is the critical point beyond which the hydrodynamics are controlled by the fluid oscillation. Also, detailed examinations of single-bubble breakage and residence time in an OBC above the critical oscillation level would allow one to distinguish the different mechanisms controlling the bubble size and the gas holdup. Despite the simplicity of the approach presented here, we believe that, compared to the purely empirical correlations used for scaling purposes, it is a significant improvement in the characterization of the gas-liquid dispersion in an OBC.

Acknowledgments

M. S. N. Oliveira wishes to acknowledge Fundação para a Ciência e Tecnologia and Heriot-Watt University for financial support. The authors would also like to thank Mr. Benoit Saye for the help with the bubble size measurements and Dr. Andrew Fitch for providing the liquid flow maps that allowed for the calculation of vorticity. Special thanks are due to Prof. Früh for valuable discussions and comments.

Literature Cited

Baird, M. H. I., and J. H. Garstang, "Gas Absorption in a Pulsed Bubble Column," *Chem. Eng. Sci.*, **27**, 823 (1972).

Baird, M. H. I., and S. J. Lane, "Drop Size and Holdup in a Reciprocating Plate Extraction Column," *Chem. Eng. Sci.*, **28**, 947 (1973).

Baird, M. H. I., and N. V. Rama Rao, "Characteristics of a Countercurrent Reciprocating Plate Bubble Column. 2. Axial Mixing and Mass Transfer," *Can. J. of Chem. Eng.*, **66**, 222 (1988).

Baird, M. H. I., and N. V. Rama Rao, "Power Dissipation and Flow Patterns in Reciprocating Baffle-Plate Columns," *Can. J. of Chem. Eng.*, **73**, 417 (1995).

Baird, M. H. I., and P. Stonestreet, "Energy Dissipation in Oscillatory Flow within a Baffled Tube," *Trans. IChemE*, **73**, 503 (1995).

Baird, M. H. I., and N. V. Rama Rao and P. Stonestreet, "Power Dissipation and Holdup in a Gassed Baffle-Plate Column," *Trans. IChemE*, **74**, 463 (1996).

Batchelor, G. K., "Chapter 6: The Universal Equilibrium Theory," *The Theory of Homogeneous Turbulence*, Cambridge University Press (1953).

Bhavaraju, S. M., T. W. F. Russel, and H. W. Blanch, "The Design of Gas Sparged Devices for Viscous Liquid Systems," *AIChE J.*, **24**, 454 (1978).

Brunold, C. R., J. C. B. Hunns, M. R. Mackley, and J. W. Thompson, "Experimental Observations on Flow Patterns and Energy Losses for Oscillatory Flow in Ducts Containing Sharp Edges," *Chem. Eng. Sci.*, **44**, 1227 (1989).

Calderbank, P. H., "Physical Rate Processes in Industrial Fermentation, Part 1: The Interfacial Area in Gas-Liquid Contacting with Mechanical Agitation," *Tran. IchemE*, **36**, 443 (1958).

Calderbank, P. H., and M. B. Moo-Young, "The Mass-Transfer Efficiency of Distillation and Gas-Absorption Plate Columns. Part 2: Liquid-Phase Mass-Transfer Coefficients in Sieve-Plate Columns," *Int. Symp. on Distillation*, Brighton, IChemE, London, 59 (1960).

Clift, R., J. R. Grace, and M. E. Weber, *Bubbles, Drops and Particles*, Academic Press (1978).

Fitch, A. W., "Characterisation of Flow in an Oscillatory Baffled Column Using Digital Particle Image Velocimetry and Laser Induced Fluorescence, " PhD Thesis, School of Engineering and Physical Sciences, Chemical Engineering, Heriot-Watt University, Edinburgh, U.K. (2003).

Fung, J. C. H., "Gravitational Settling of Particles and Bubbles in Homogeneous Turbulence," *J. of Geophysical Research*, **98**, 20287 (1993).

Godfrey, J. C., and M. J. Slater, "Slip Velocity Relationships for Liquid-Liquid Extraction Columns," *Trans. IChemE*, **69**, 130 (1991).

Hafez, M. M., and M. H. I. Baird, "Power Consumption in a Reciprocating Plate Extraction Column," *Trans. IChemE*, **56**, 229 (1978).

Hesketh, R. P., A. W. Etchells, and T. W. F. Russell, "Experimental Observations of Bubble Breakage in Turbulent Flow," *Ind. Eng. Chem. Res.*, **30**, 835 (1991).

Hewgill, M. R., M. R. Mackley, A. B. Pandit, and S. S. Pannu, "Enhancement of Gas-Liquid Mass Transfer Using Oscillatory Flow in a Baffled Tube," *Chem. Eng. Sci.*, **48**, 799 (1993).

Hinze, J. O., "Fundamentals of the Hydrodynamic Mechanism of Splitting in Dispersion Processes," *AIChE J.*, **1**, 289 (1955).

Houghton, G., "The Behaviour of Particles in a Sinusoidal Velocity Field," *Proc. Royal Soc.*, **A 272**, 33 (1963).

Howes, T., and M. R. Mackley, "Experimental Axial Dispersion for Oscillatory Flow through a Baffled Tube," *Chem. Eng. Sci.*, **45**, 1349 (1990).

Howes, T., M. R. Mackley, and E. P. L. Roberts, "The Simulation of Chaotic Mixing and Dispersion for Periodic Flows in Baffled Channels," *Chem. Eng. Sci.*, **46**, 1669 (1991).

Jakobsen, H. A., B. H. Sannaes, S. Grevskott, and H. F. Svendsen, "Modeling of Vertical Bubble-Driven Flows," *Ind. and Eng. Chem. Res.*, **36**, 4052 (1997).

Jealous, A. C., and H. F. Johnson, "Power Requirements for Pulse Generation in Pulse Columns," *Industrial and Eng. Chem.*, **47**, 1159 (1955).

Karabelas, A. J., "Droplets Size Spectra Generated in Turbulent Pipe Flow of Dilute Liquid/Liquid Dispersions," *AIChE J.*, **24**, 170 (1978).

Kawase, Y., and M. B. Moo-Young, "Mathematical Models for Design of

Bioreactors: Applications of Kolmogoroff's Theory of Isotropic Turbulence," *Chem. Eng. J.*, **43**, B19 (1990).
Knott, G. F., and M. R. Mackley, "On Eddy Motions near Plates and Ducts, Induced by Water Waves and Periodic Flows," *Philosophical Trans. of the Royal Society*, **294**, 599 (1980).
Kolmogoroff, A., "The Local Structure of Turbulence in Incompressible Viscous Fluid for Very Large Reynolds Numbers," *(Doklady) Académie Sciences, USSR*, **30**, 301 (1941).
Kolmogoroff, A., "On the Disintegration of Drops in a Turbulent Flow," *(Doklady) Akad. Nauk. USSR*, **66**, 825 (1949).
Mackley, M. R., and X. Ni, "Mixing and Dispersion in a Baffled Tube for Steady Laminar and Pulsatile Flow," *Chem. Eng. Sci.*, **46**, 3139 (1991).
Mackley, M. R., K. B. Smith, and N. P. Wise, "The Mixing and Separation of Particle Suspensions Using Oscillatory Flow in Baffled Tubes," *Trans. IChemE*, **71**, 649 (1993).
Magnaudet, J., and I. Eames, "The Motion of High-Reynolds-Number Bubbles in Inhomogeneous Flows," *Ann. Rev. Fluid Mech.*, **32**, 659 (2000).
Ni, X., and M. R. Mackley, "Chemical Reaction in a Batch Pulsatile Flow and Stirred Tank Reactors," *Chem. Eng. J.*, **52**, 107 (1993).
Ni, X., S. Gao, R. H. Cumming, and D. W. Pritchard, "A Comparative Study of Mass Transfer in Yeast for a Batch Pulsed Baffled Bioreactor and a Stirred Tank Fermenter," *Chem. Eng. Sci.*, **50**, 2127 (1995a).
Ni, X., S. Liu, M. J. Joyce, P. S. Grewal, and C. A. Greated, "A Study of Velocity Vector Profile and Strain Rate Distribution for Laminar and Oscillatory Flows in a Baffled Tube Using Particle Image Velocimetry," *J. of Flow Visualization and Image Proc.*, **2**, 135 (1995b).
Ni, X., Y. Zhang, and I. Mustafa, "An Investigation of Droplet Size and Size Distribution in Methylmethacrylate Suspensions in a Batch Oscillatory-Baffled Reactor," *Chem. Eng. Sci.*, **53**, 2903 (1998).
Ni, X., M. R. Mackley, A. P. Harvey, P. Stonestreet, M. H. I. Baird, and N. V. Rama Rao, "Mixing through Oscillations and Pulsations - A guide to Achieving Process Enhancements in the Chemical and Process Industries," *Trans IChemE*, **81**(Part A), 373 (2003a).
Ni, X., H. Jian, and A.W. Fitch, "Evaluation of Turbulent Integral Length Scale in an Oscillatory Baffled Column using Large Eddy Simulation and Digital Particle Image Velocimetry," *Trans. IChemE*, **81** (A8), 842 (2003b).
Odar, F., and W. S. Hamilton, "Forces on a Sphere Accelerating in a Viscous Fluid," *J. of Fluid Mech.*, **18**, 302 (1964).
Oliveira, M. S. N., and X. Ni, "Gas Hold-up and Bubble Diameters in a Gassed Oscillatory Baffled Column," *Chem. Eng. Sci.*, **56**, 6143 (2001).
Oliveira, M. S. N., A. W. Fitch, and X. Ni, "A Study of Velocity and Residence Time of Single Bubbles in a Gassed Oscillatory Baffled Column: Effect of Oscillation Amplitude," *J. of Chem. Technol. and Biotechnol.*, **78**, 220 (2003a).
Oliveira, M. S. N., A. W. Fitch, and X. Ni, "A Study of Bubble Velocity and Bubble Residence Time in a Gassed Oscillatory Baffled Column: Effect of Oscillation Frequency," *Trans. IChemE*, **81**, 233 (2003b).
Oliveira, M. S. N., *Characterisation of a Gas-Liquid Oscillatory Baffled Column*, PhD thesis, School of Engineering and Physical Sciences, Chemical Engineering, Heriot-Watt University, Edinburgh, U.K. (2003).
Oliveira, M. S. N., and X. Ni, "The eEffect of Hydrodynamics on Mass Transfer in a Gas-Liquid Oscillatory Baffled Column," *Chem. Eng. J.*, **99**, 59 (2004).
Panton, R. L., and A. L. Goldman, "Correlation of Nonlinear Orifice Impedance," *J. Acoustic Soc. of America*, **60**, 1390 (1976).
Parthasarathy, R., and N. Ahmed, "Size Distribution of Bubbles Generated by Fine-Pore Spargers," *J. of Chem. Eng. of Japan*, **29**, 1030 (1996).
Risso, F., and J. Fabre, "Oscillations and Breakup of a Bubble Immersed in a Turbulent Field," *J. of Fluid Mech.*, **372**, 323 (1998).
Risso, F., "The Mechanisms of Deformations and Breakup of Drops and Bubbles," *Multiphase Sci. and Technol.*, **12**, 1 (2000).
Roberts, E. P. L., and M. R. Mackley, "The Development of Asymmetry and Period Doubling for Oscillatory Flow in Baffled Channels," *J. of Fluid Mech.*, **328**, 19 (1996).
Schügerl, K., "New Bioreactors for Aerobics Processes," *Int. Chem. Eng.*, **22**, 591 (1982).
Sene, K. J., J. C. R. Hunt, and N. H. Thomas, "The Role of Coherent Structures in Bubble Transport by Turbulent Shear Flows," *J. of Fluid Mech.*, **259**, 219 (1994).
Shinnar, R., "On the Behaviour of Liquid Dispersions in Mixing Vessels," *J. of Fluid Mech.*, **10**, 259 (1961).
Sprow, F. B., "Drop Size Distributions in Strongly Coalescing Agitated Liquid-Liquid Systems," *AIChE J.*, **13**, 995 (1967).
Stephanoff, K. D., I. J. Sobey, and B. J. Bellhouse, "On Flow through Furrowed Channels. Part 2. Observed Flow Patterns," *J. of Fluid Mech.*, **96**, 27 (1980).
Thomas, R. M., "Bubble Coalescence in Turbulent Flows," *Int. J. of Multiphase Flow*, **7**, 709 (1981).
Tooby, P. F., G. L. Wick, and J. D. Isaacs, "The Motion of a Small Sphere in a Rotating Velocity Field: A Possible Mechanism for Suspending Particles in Turbulence," *J. of Geophy. Res.*, **82**, 2096 (1977).
Tsouris, C., and L. L. Tavlarides, "Breakage and Coalescence Models for Drops in Turbulent Dispersions," *AIChE J.*, **40**, 395 (1994).
Zakrzewski, W., J. Lippert, A. Lübbert, and K. Schügerl, "Investigation of the Structure of 2-Phase Flows in Bubble Column Bioreactors. 6. Turbulence Structures," *Euro. J. of Appl. Microbiology and Biotechnol.*, **12**, 150 (1981).
Zhang, Y., X. Ni, and I. Mustafa, "A Study of Oil-Water Dispersion in a Pulsed Baffled Reactor," *J. of Chem. Technol. and Biotechnol.*, **66**, 305 (1996).

Appendix

In order to estimate the average bubble rise velocity in the OBC, a simplified model based on the balance of forces acting on a single bubble was developed. In the interest of simplicity, the force balance was performed in the vertical (axial) direction only. Four main forces were considered: bubble and liquid inertia (F_{BI} and F_{LI}, respectively), buoyancy (F_B) and drag forces (F_D).

The force due to the inertia of the bubble can be expressed as

$$F_{BI} = (\rho_G + a_m \rho_L) V_B \frac{dU_R(t)}{dt} \quad \text{(N)} \tag{A1}$$

where ρ_G is the density of the dispersed phase (kg m^{-3}), V_B is the volume of the bubble (m^3), $U_R(t)$ the time-dependent velocity (m s^{-1}) of the bubble relative to the liquid [U_R (t) = $U_B(t) - U_L$ (t)], $U_B(t)$ the velocity of the bubble (m s^{-1}), $U_L(t)$ the velocity of the liquid (m s^{-1}) and a_m the added mass coefficient. The added mass term reflects the acceleration of the displaced fluid in the neighborhood of the bubble. The buoyancy force is given by

$$F_B = (\rho_L - \rho_G) V_B g \quad \text{(N)} \tag{A2}$$

The dynamic pressure force caused by liquid inertia on the bubble can be expressed as

$$F_{LI} = \rho_L V_B \frac{dU_L(t)}{dt} \quad \text{(N)} \tag{A3}$$

The bubble experiences a resistance to motion through the fluid, called the drag force, which is exerted by the liquid on the moving bubble. This force depends on the relative velocity between the phases (Odar and Hamilton, 1964), as follows

$$F_D = \frac{C_D}{2} \rho_L A_B U_R(t) |U_R(t)| \quad \text{(N)} \tag{A4}$$

where C_D is the drag coefficient. The drag coefficient depends on the flow regime and the liquid properties. When D_B is larger

than 1.3 mm, C_D can be evaluated from Eq. A5 (Jakobsen et al., 1997)

$$C_D = \frac{1}{0.378 + \dfrac{1.605\sigma}{\rho_L g D_B^2}} \tag{A5}$$

where σ is the air-water surface tension (kg s^{-2}). The use of the absolute value, $|U_R(t)|$, in Eq. A4 ensures that the drag force always acts in the opposite direction to the relative velocity of the bubble.

Considering the forces as described earlier, the general force balance is simply

$$F_{BI} = F_B - F_D + F_{LI} \tag{A6}$$

It is worth noting here that the drag forces have been assumed to be of the same nature as those in steady motion. This is equivalent to neglecting the Basset force, a transient component of the drag force that allows for the effect of deviations of the flow pattern around the bubble from that at steady state. The Basset force cannot be evaluated theoretically, except for very small spherical bubbles (Houghton, 1963). Furthermore, following Magnaudet and Eames (2000), this term may be neglected, with respect to the other forces in the balance, for bubbles in oscillatory flow.

For an air-water system, $\rho_L \gg \rho_G$, and the terms associated with ρ_G can be ignored. Thus, substituting the earlier expressions, the general force balance becomes

$$\frac{dU_R(t)}{dt} = \frac{g}{a_m} - \frac{3}{4a_m D_B\left(0.378 + \dfrac{1.605\sigma}{\rho_L g D_B^2}\right)} \times U_R(t)|U_R(t)| + \frac{1}{a_m}\frac{dU_L(t)}{dt} \tag{A7}$$

The liquid oscillatory velocity can be defined as

$$U_L(t) = x_o \omega \sin(\omega t) \tag{A8}$$

This expression is based on the cross-section of the entire column, and assumes the column to be free of baffles. However, the presence of baffles in the OBC causes a constriction to the passage of the fluid, which significantly increases the local velocity. In light of this, it is more accurate to use the maximum instantaneous liquid velocity, which is observed in the vicinity of the constriction. This can be achieved by replacing the amplitude of oscillation in Eq. A8 by a "corrected amplitude" (x_o'), given by

$$x_o' = \frac{x_o}{C_o \alpha} \tag{A9}$$

In doing so, the effect of the constriction is accounted for in the calculations. Using this correction and substituting Eq. A8 in Eq. A9, considering that $U_R(t) = U_B(t) - x_o'\omega \sin(\omega t)$, one obtains Eq. 22.

Manuscript received July 28, 2003, and revision received Mar. 15, 2004.